View metadata, citation and similar papers at core.ac.uk
brought to you by CORE
provided by NASA Technical Reports Server

Development of a Geomagnetic Storm Correction to the International Reference Ionosphere E-Region Electron Densities Using TIMED/SABER Observations

C. J. Mertens[a], X. Xu[b], J. R. Fernandez[a], D. Bilitza[c], J. M. Russell III[d], and M. G. Mlynczak[a]

a NASA Langley Research Center, Hampton, VA USA
b SSAI, Inc., Hampton, VA, USA
c George Mason University, Fairfax, VA USA
d Hampton University, Hampton, VA USA

ABSTRACT

Auroral infrared emission observed from the TIMED/SABER broadband 4.3 um channel is used to develop an empirical geomagnetic storm correction to the International Reference Ionosphere (IRI) E-region electron densities. The observation-based proxy used to develop the storm model is SABER-derived $NO^+(v)$ 4.3 um volume emission rates (VER). A correction factor is defined as the ratio of storm-time $NO^+(v)$ 4.3 um VER to a quiet-time climatological averaged $NO^+(v)$ 4.3 um VER, which is linearly fit to available geomagnetic activity indices. The initial version of the E-region storm model, called STORM-E, is most applicable within the auroral oval region. The STORM-E predictions of E-region electron densities are compared to incoherent scatter radar electron density measurements during the Halloween 2003 storm events. Future STORM-E updates will extend the model outside the auroral oval.

1. INTRODUCTION

Infrared emission observed by the Sounding of the Atmosphere using Broadband Emission Radiometry (SABER) instrument, launched onboard the Thermosphere-Ionosphere-Mesosphere-Energetics and Dynamics (TIMED) satellite in 2001, are providing significant new insight into the ionosphere-thermosphere solar-geomagnetic storm response. Specifically, several orders of magnitude enhancement in the nighttime SABER 4.3 um limb radiance channel measurements (2290-2405 cm^{-1}) have been observed during strong geomagnetic storms. SABER observations and data analysis revealed that nighttime 4.3 um radiance is dominated by $NO^+(v)$ rotation-vibration band emission during geomagnetically disturbed conditions [*Mertens et al.,* 2009a-b, 2008, 2007a-b]. During solar-geomagnetic storms, auroral particle precipitation increases the ionization of the neutral atmosphere, producing vibrationally excited NO^+ (i.e., $NO^+(v)$) through fast exothermic ion-neutral chemical reactions, which emits in the 4.3 um spectral region [*Mertens et al.,* 2008, 2007a]. Since NO^+ is the terminal E-region ion, by charge neutrality, $NO^+(v)$ 4.3 um emission is also an excellent proxy suitable for deriving an empirical model of storm-time enhancements to the E-region electron densities [*Fernandez et al.,* 2009; *Mertens et al.,* 2007a-b]. Thus, $NO^+(v)$ 4.3 um volume emission rates (VER) are the observation-based data product used to develop the empirical model.

The International Reference Ionosphere (IRI) is a widely used data-based model for the specification of ionospheric parameters and is recommended for international use by the Committee on Space Research (COSPAR) and the International Union of Radio Science (URSI) [*Bilitza*, 2001]. However, the specification of the ionospheric response to solar-geomagnetic

disturbances in IRI remains largely incomplete, and there is currently no storm-time correction to IRI parameters in the E-region. Ratios of storm-time $NO^+(v)$ 4.3 um VER to quiet-time climatological $NO^+(v)$ 4.3 um VER, fit to available geomagnetic activity indices, is used to correct the IRI E-region electron density peak concentration for geomagnetic storm enhancements.

The empirical model described in this paper is called STORM-E. The initial version of STORM-E adjusts the E-region electron density peak concentration for geomagnetic activity and is best suited for the auroral oval region, which is described in section 2. STORM-E adjustments to the IRI E-region electron densities are compared to incoherent scatter radar (ISR) electron density measurements in section 3 for the Halloween 2003 storm events. Summary and conclusions are given in section 4.

2. STORM-E PARAMETERIZATION

The STORM-E geomagnetic activity correction factor is defined as a storm-to-quiet ratio (SQR) of $NO^+(v)$ 4.3 um VER, such that

$$r(z,\lambda_m,\varphi_m,t)=\frac{VER_{\text{Storm}}(z,\lambda_m,\varphi_m,t)}{VER_{\text{Quiet}}(z,\lambda_m,\varphi_m)}. \tag{1}$$

In the above equation, VER denotes $NO^+(v)$ VER derived from nighttime SABER 4.3 um limb radiance measurements [*Mertens et al.,* 2007a, 2008]; z, λ_m, φ_m, and t refer to altitude (km), magnetic latitude (degrees), magnetic longitude (degrees), and UT-time (hrs), respectively. The reason for introducing a correction factor such as defined in (1) is the observation that

$$r \approx \frac{[NO^+]_{\text{Storm}}}{[NO^+]_{\text{Quiet}}} \approx \frac{[e]_{\text{Storm}}}{[e]_{\text{Quiet}}}, \tag{2}$$

where $[e]$ is the electron density. Equations (1) and (2) represent the fundamental basis of STORM-E, which state that the geomagnetic storm enhancement to the E-region electron density can be well approximated by SABER-derived $NO^+(v)$ 4.3 um VER SQR. An initial validation of the above equations was presented by *Mertens et al.* [2008] by comparing SABER $NO^+(v)$ 4.3 um VER SQR with a coincidence measurement of ISR electron density SQR at Tromso, Norway during the Halloween 2003 storm period. Recently, *Fernandez et al.* [2009] extended this validation study by comparing SABER/ISR SQR at other geographic locations and for other storm events. The comparisons show remarkable agreement over a wide range of weak to strong geomagnetic storm activity.

The initial version of STORM-E provides a geomagnetic storm enhancement factor to scale the nominal IRI E-region electron density peak concentration for geomagnetic storm activity, i.e.,

$$[NmE(t)]^{\text{IRI}}_{\text{Storm}}(\text{peak}) = \tilde{r}(\lambda_m,t) \times [NmE]^{\text{IRI}}_{\text{Nominal}}(\text{peak}). \tag{3}$$

As the above equation indicates, the storm-induced enhancement to the nominal IRI E-region electron density peak concentration is obtained by an altitude-averaged $NO^+(v)$ 4.3 um VER SQR, such that

$$\tilde{r}(\lambda_m, t) = \frac{1}{\Delta z} \int_{Z_B}^{Z_T} r(z, \lambda_m, t) dz. \tag{4}$$

The STORM-E geomagnetic correction factor defined in (3) and (4) is computed as follows. The $NO^+(v)$ 4.3 um VER data from years 2002-2006 are sorted roughly according to season based on the SABER yaw cycles [see *Fernandez et al.,* 2009]. The VER data are interpolated to a uniform altitude grid and further sorted into 5-degree magnetic latitude bins and 3-hour UT-time bins. The purpose of sorting the VER data into time bins is to associate the time-averaged VER data with a geomagnetic activity index. To calculate the climatological averages, or the VER_{Quiet} in (1), all $NO^+(v)$ 4.3 um VER profiles from 2002-2006 with $kp \leq 3$ are averaged at each altitude and within each magnetic latitude bin and for each season. The altitude-dependent SQR under the integral sign in (4) is computed by dividing each time-averaged $NO^+(v)$ 4.3 um VER profile from 2002-2006 by the corresponding climatological average for each season and magnetic latitude bin. The altitude-independent SQR, i.e., the geomagnetic correction factor in (3), is calculated according to (4) with bottom (Z_B) and top (Z_T) altitudes given by 116 km and 120 km, respectively. This altitude range was chosen because of the consistent good agreement between SABER/ISR SQR [*Fernandez et al.,* 2009], which can be explained in terms of the error budgets of both measurement techniques.

The next step in STORM-E development is to fit the SQR to a polynomial in a geomagnetic forcing parameter (G); thus,

$$\tilde{r}(\lambda_m, t) = \sum_{i=0}^{N} c_i(\lambda_m) G^i(\lambda_m, t), \tag{5}$$

where c_i are the polynomial expansion coefficients and G^i is the geomagnetic forcing parameter to the *ith* power. The forcing parameter (G) captures the dynamical response of the E-region electron density peak concentration to geomagnetic activity. Assuming a linear impulse-response, the geomagnetic forcing parameter can be expressed as a convolution of an external geomagnetic driver index (D) with a dynamical response function ($F(\tau)$), where

$$G(\lambda_m, t) = \int_{-T_S}^{T} F(\lambda_m, \tau) D(t - \tau) d\tau. \tag{6}$$

The effective memory of the storm-time response corresponds to time T in the upper limit of the integral in (6). The lower limit of the integral (T_S) represents the start time and is chosen to ensure numerical stability in solving for the response function ($F(\tau)$) [*Vassiliadis et al.*, 2002]. The use of linear impulse-response theory has been successfully applied to developing an empirical storm-time correction model to adjust the nominal IRI F-region critical frequency [*Fuller-Rowell et al.,* 2000; *Araujo-Pradere et al.,* 2002, 2003, 2004].

The geomagnetic driver indices (D) in (6) must be widely used and readily accessible geomagnetic activity indices for practical implementation in IRI. The indices considered in this work are the Ap, Hemispheric Power (HP), Disturbed Storm Time (Dst), and the Auroral Electrojet (AE) indices.

Considerable guidance into the form of the response function in (6) can be obtained by examining the cross correlation function between $NO^+(v)$ 4.3 um VER and the geomagnetic activity indices (see *Mertens et al.* [2007b] and *Fernandez et al.* [2009]). For example, Figure 1 shows the cross correlation between $NO^+(v)$ 4.3 um VER and HP for a period of strong geomagnetic activity during the Halloween 2003 storm events.

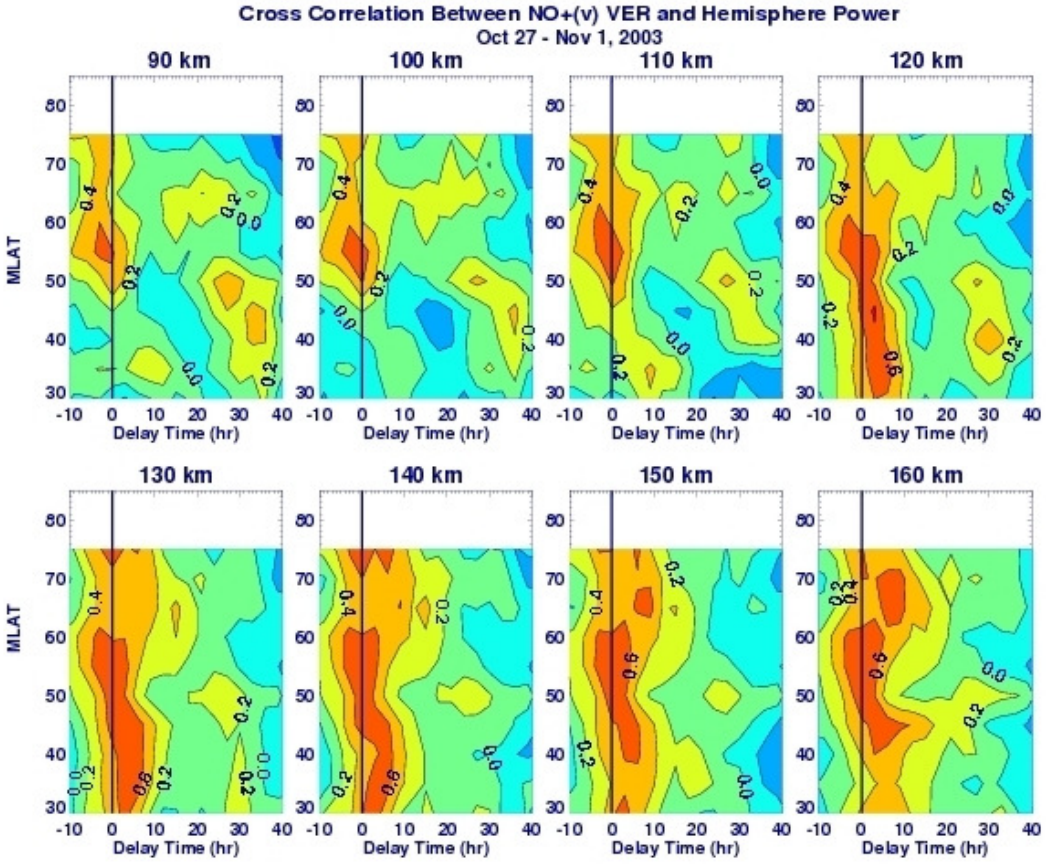

Figure 1: Cross correlation between SABER-derived $NO^+(v)$ 4.3 um VER and Hemispheric Power (denoted HP: unit is GW) index derived from NOAA/POES satellites. Each panel shows the cross correlation as a function of magnetic latitude (degrees) and delay time (hours). The different panels correspond to different altitudes. The cross correlation function is defined in Vassiliadis et al. [2002].

Figure 1 shows that $NO^+(v)$ 4.3 um VER responds nearly instantaneously (i.e., zero delay time) to auroral particle precipitation measured by the HP index and is geographically concentrated in the auroral oval region at altitudes below 120 km. At altitudes above 120 km, significant storm-time enhancements in $NO^+(v)$ 4.3 um VER occur equatorward of the auroral oval with a time delay of 3-6 hours. Evidence (not shown or discussed here) suggests that the $NO^+(v)$ 4.3 um VER enhancements at mid- and low-latitudes are due to NO transport out of the auroral zone followed by $O_2^+ + NO$ charge transfer that leads to $NO^+(v)$ excitation and 4.3 um emission [see *Mertens et al.,* 2008]. The morphology of the cross correlations between $NO^+(v)$ 4.3 um VER and the other geomagnetic activity indices considered – i.e., Ap, Dst, and AE – are similar to Figure 1.

The initial goal of STORM-E is to provide an empirical geomagnetic storm correction to the E-region electron density peak concentrations. Since the peak is located at an altitude below 120 km, Figure 1 suggests the response function can be approximated by a delta function in the delay time (δ), i.e.,

$$F(\lambda_m, \tau) \sim \delta(\tau). \tag{7}$$

Furthermore, scatter plots shown in Figure 2 suggests that storm-time SQR varies nearly linearly with the geomagnetic activity indices. Combining these observations with (7), the STORM-E parameterization in the auroral zone can be approximated by

$$\tilde{r}(\lambda_m, t) \approx a(\lambda_m) + b(\lambda_m) D(t). \tag{8}$$

The coefficients $a(\lambda_m)$ and $b(\lambda_m)$ are determined for each magnetic latitude bin (λ_m), for each season, and for each geomagnetic activity index by linearly fitting the seasonal-altitude-averaged SQR ($\tilde{r}(\lambda_m, t)$) to each geomagnetic activity index.

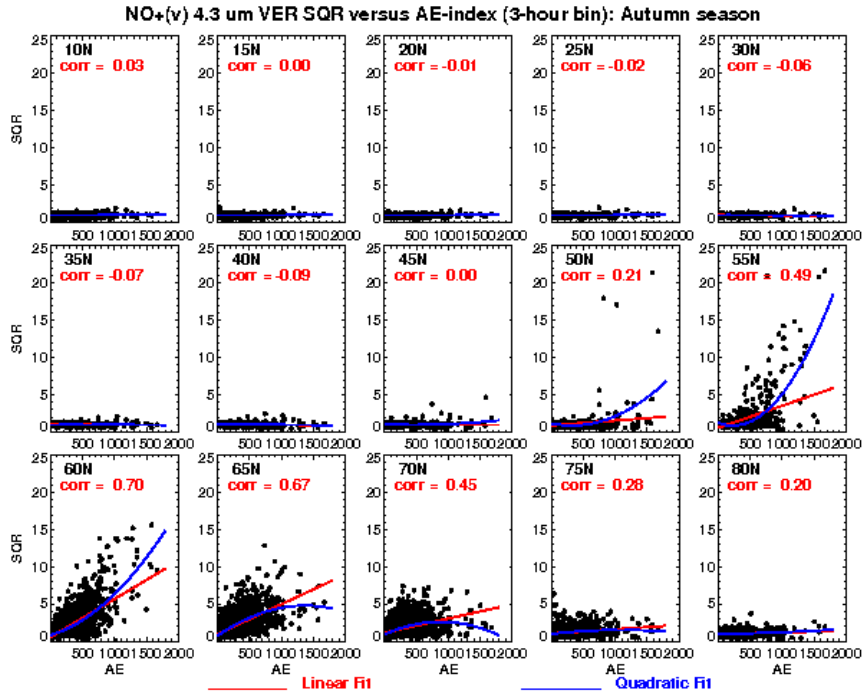

Figure 2: Scatter plots of $NO^+(v)$ 4.3 um VER SQR versus AE-index for +/- 2.5-degree magnetic latitude bins from 10N to 80N for the autumn season. Each data point represents a 3-hour UT-time average of both SQR and AE. The red lines are linear fits to the SQR/AE data points and the linear correlation coefficient is denoted "corr" in red. The blue lines are quadratic fits to the SQR/AE data points.

Figure 2 shows SQR versus AE-index scatter plots at different magnetic latitude bins for the autumn season (~ September –November for years 2002-2006). The figure shows no storm-time

$NO^+(v)$ 4.3 um VER enhancements (i.e., $\tilde{r} > 1$) at latitudes equatorward of 50N, which is consistent with the results shown in Figure 1 for VER enhancements at altitudes less than 120 km. Recall that SQR is altitude-averaged from 116 km to 120 km to provide a storm-time correction to the E-region electron density peak concentration. The largest SQR enhancements shown in Figure 2 occur in the auroral oval region between 55N and 65N, also consistent with the results shown in Figure 1. The linear correlation coefficient between SQR and the AE-index is between 0.50 and 0.67 in the auroral oval region. The scatter plots between SQR and the Ap, HP, and Dst indices are similar to Figure 2. However, the largest linear correlation coefficient occurs between SQR and the AE-index.

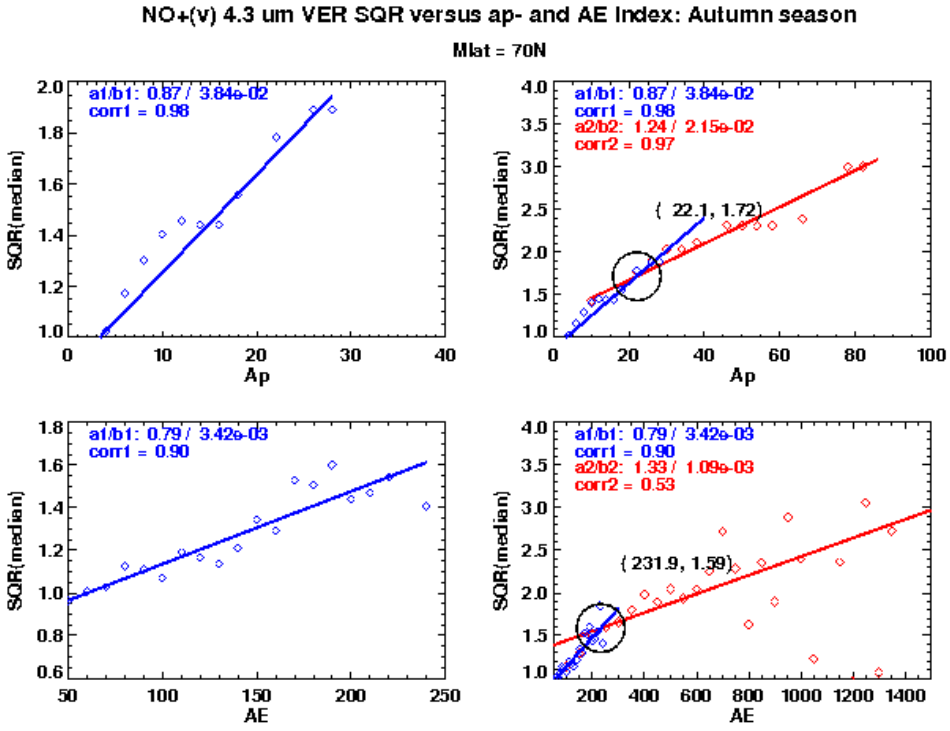

Figure 3: Scatter plot of $NO^+(v)$ 4.3 um VER SQR versus Ap and AE indices for the 70N magnetic latitude bin. This figure was produced by sorting the SQR into Ap and AE index bins and computing the median SQR in each index bin. The left column shows the scatter plots for low geomagnetic activity. The ap-index bin size is 2 and the AE-index bin size is 10 for the left column. The right column shows the merging of two linear fits for low (blue) and high (right) geomagnetic activity. The bins sizes for high activity are 4 for the Ap-index and 50 for the AE-index. The merge coordinates (index, SQR) are indicated in the right column panels. The fit coefficients from (8) and linear correlation coefficient for the fits are given in the legend.

Figure 2 indicates small nonlinearities in the SQR/AE scatter data near the auroral oval region. However, a simple quadratic fit to the SQR/AE data doesn't provide a satisfactory fit. A better approach is to further average the SQR into broader geomagnetic index bins. An example is shown in Figure 3 for the Ap-index and AE-index at the 70N magnetic latitude bin. The

advantage of this approach is twofold: (1) the nonlinearity can be approximated by splicing two linear fits, and (2) the linear correlation between SQR and the geomagnetic index increases. A similar technique was applied to the HP and Dst indices and at the other magnetic latitudes.

3. HALLOWEEN 2003 STORM RESULTS

The initial STORM-E parameterization described in the previous section is tested by comparing ISR electron density measurements during the Halloween 2003 storm events with nominal IRI E-region electron densities scaled by STORM-E to account for geomagnetic activity enhancements. The ISR measurements are taken from three high-latitude locations: (1) EISCAT VHF data at Tromso, Norway (magnetic: 67N, 116E), (2) Lonyearsbyen, Norway ISR data (magnetic: 74N, 129E), and (3) Sondrestrom, Greenland ISR data (magnetic: 76N, 36E). For the comparisons, IRI/ISR electron densities were averaged in altitude from 116 km to 120 km. To test the relative accuracy of STORM-E, the nominal quiet-time IRI electron density was scaled to agree with the quiet-time average of the ISR measurements at 118 km, midway between 116 km and 120 km.

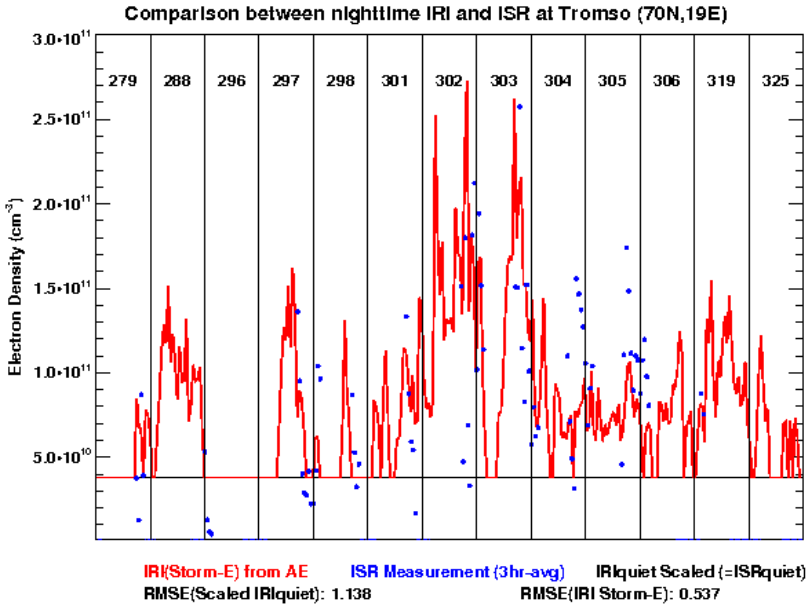

Figure 4: Comparison between ISR electron density measurements at Tromso, Norway and quiet-time IRI adjusted for geomagnetic activity using STORM-E driven by the AE-index during the Halloween 2003 storm period. The day of year is indicated in the figure. The IRI/ISR electron densities have been altitude averaged from 116 km to 120 km. The quiet-time IRI electron density was scaled to agree with the quiet-time average ISR electron density at 118 km, which is indicated by the black horizontal line.

Figure 4 shows a comparison between ISR measurements at Tromso, Norway and IRI adjusted by STORM-E. The comparisons are shown for all the available storm-time ISR data at Tromso during the Halloween 2003 storm period. The STORM-E parameterization for this comparison is from the 70N magnetic latitude bin. In Figure 4, STORM-E is driven by the AE-index. The black horizontal line represents the nominal quiet-time IRI electron density. STORM-E provides a significant improvement in capturing the dynamical response of the E-region electron density with geomagnetic activity. STORM-E driven by HP, Ap, and Dst indices provide significant improvements as well, but STORM-E driven by AE yields the best comparison with Tromso ISR measurements.

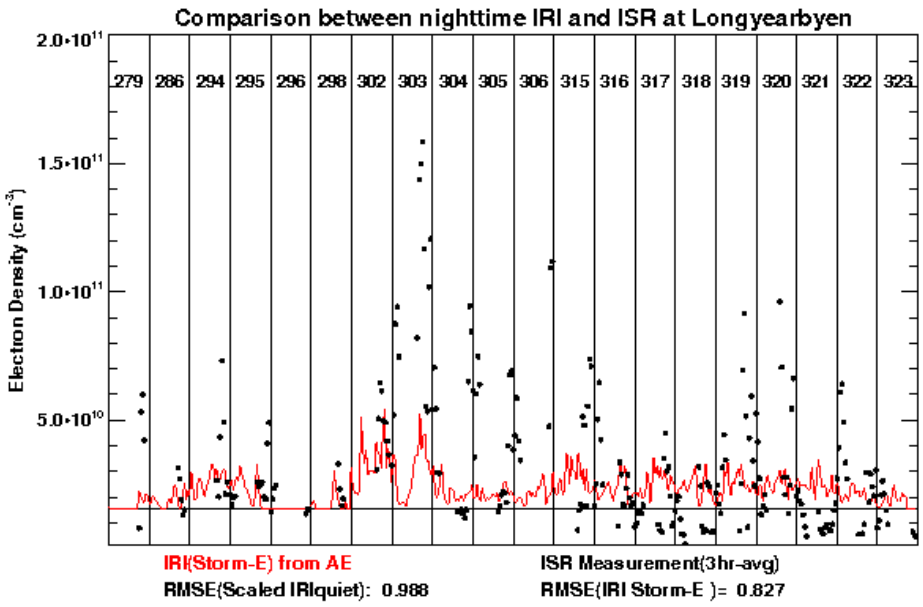

Figure 5: Comparison between ISR electron density measurements at Longyearsbyen, Norway and quiet-time IRI adjusted for geomagnetic activity using STORM-E driven by the AE-index during the Halloween 2003 storm period. The day of year is indicated in the figure. The IRI/ISR electron densities have been altitude averaged from 116 km to 120 km. The quiet-time IRI electron density was scaled to agree with the quiet-time ISR electron density at 118 km, which is indicated by the black horizontal line.

Figures 5 and 6 show comparisons between IRI adjusted by STORM-E and ISR measurements at Longyearsbyen, Norway and Sondrestrom, Greenland, respectively. The comparisons are shown for all the available storm-time Longyearsbyen and Sondrestrom ISR data during the Halloween 2003 storm period. The STORM-E parameterization for these comparisons is from the 75N magnetic latitude bin and is driven by the AE-index. The black horizontal lines in Figures 5 and

6 indicate the nominal quiet-time IRI electron densities. While STORM-E improves the prediction of storm-time E-region electron densities over the nominal quiet-time IRI result, the improvement is not nearly as good as the comparisons at Tromso. The same holds true for STORM-E driven by the HP, Ap, and Dst indices, with the AE-index giving the best comparison to ISR measurements.

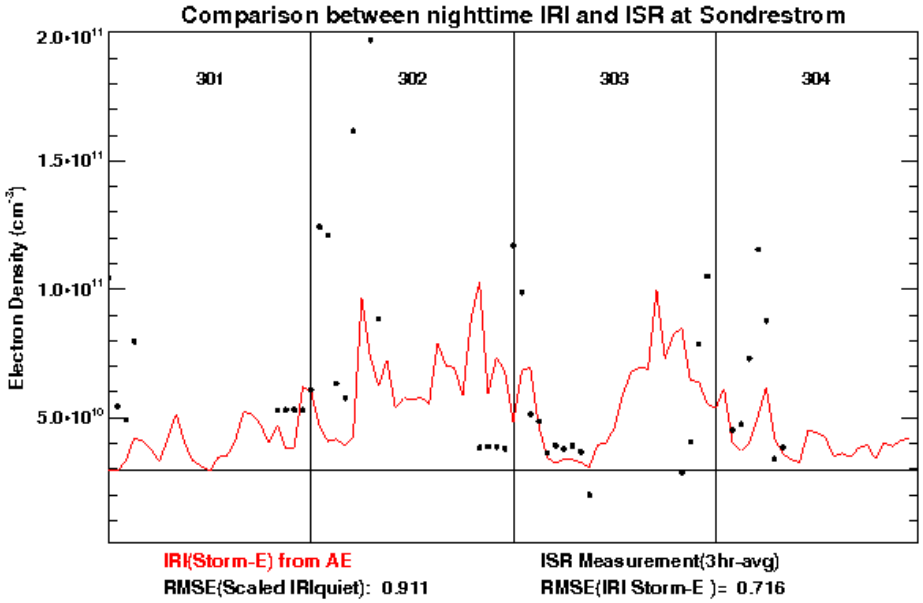

Figure 6: Comparison between ISR electron density measurements at Sondrestrom, Greenland and quiet-time IRI adjusted for geomagnetic activity using STORM-E driven by the AE-index during the Halloween 2003 storm period. The day of year is indicated in the figure. The IRI/ISR electron densities have been altitude averaged from 116 km to 120 km. The quiet-time IRI electron density was scaled to agree with the quiet-time ISR electron density at 118 km, which is indicated by the black horizontal line.

The smaller improvement in STORM-E geomagnetic corrections to IRI E-region electron densities at Longyearsbyen and Sondrestrom compared to Tromso is consistent with a reduction in correlation between SQR and the geomagnetic activity indices for latitudes poleward of the auroral oval region, as shown in Figure 2. The is likely due to the inadequacy of the AE, Ap, HP, and Dst indices to serve as proxies for geomagnetic activity in the polar cap region. A plausible candidate for a geomagnetic activity index at latitudes polarward of the auroral oval region is the polar cap (PC) index, which is based on ground magnetic field measurements at the near-pole Thule observatory [see *Lyatsky et al.,* 2007]. On the other hand, the use of geomagnetic indices based on ground magnetic field measurements – such as Ap, AE, Dst, and PC – can

underestimate storm-induced energy deposited in the ionosphere [*Burke et al.,* 2007]. Thus, other plausible candidate geomagnetic indices, especially for the polar cap region, are solar wind-magnetosphere-ionosphere coupling functions based on the polar cap potential and magnetospheric electric fields derived from interplanetary solar wind and magnetic field parameters [*Burke et al.,* 2007; *Lyatsky et al.,* 2007]. This is the subject of future work.

Table 1: Root-mean-square-errors (RMSE) of comparisons between ISR electron densities and nominal IRI and IRI adjusted by STORM-E electron density predictions. The IRI/ISR electron densities were averaged over the altitudes 116-120 km.

ISR Location	IRI RMSE	Storm-E RMSE				Storm-E Improvement IRI - Storm-E RMSE			
		Ap	AE	HP	Dst	Ap	AE	HP	Dst
TRO	1.138	0.626	0.537	0.992	0.693	0.512	0.601	0.546	0.445
LYR	0.988	0.862	0.827	0.833	0.881	0.126	0.161	0.155	0.107
SON	0.911	0.735	0.716	0.727	0.857	0.176	0.195	0.184	0.054

The results of the IRI/ISR comparisons are summarized in Table 1. The comparisons are quantified by computing the root-mean-sum-error (RMSE) between IRI predictions and the storm-time ISR measurements at each ISR location shown in Figures 4-6. The IRI RMSE column was computed using the nominal quiet-time IRI, scaled to agree with the average quiet-time ISR electron densities at 118 km, i.e., the horizontal lines shown in Figures 4-6. The first block of STORM-E results represent the nominal quiet-time IRI electron density scaled by the STORM-E geomagnetic correction factor. STORM-E RMSE is shown for each geomagnetic activity index. The second block of STORM-E results is indicative of the improvement in IRI predictions of storm-time E-region electron densities, as given by IRI (nominal) RMSE – IRI(storm) RMSE. The most accurate geomagnetic activity parameter used in this study for predicting storm-time E-region electron densities is the AE-index. STORM-E driven by the AE-index improved the IRI/ISR comparison by 60.1% at Tromso, 16.1% at Longyearsbyen, and 19.5% at Sondrestrom.

4. SUMMARY AND CONCLUSIONS

STORM-E is an empirical model of geomagnetic storm enhancements to E-region electron density peak concentrations. The storm-time enhancements are computed from $NO^+(v)$ VER SQR derived from TIMED/SABER broadband 4.3 um limb radiance measurements. The initial version of STORM-E is based on the following assumptions: (1) the E-region electron density responds instantaneously to geomagnetic activity, (2) the geomagnetic enhancements to E-region electron densities can be adequately parameterized by Ap, HP, AE, and Dst indices, and (3) the storm-time enhancement factor can be linearly fit to the geomagnetic activity indices previously listed. The first two assumptions imply that the initial STORM-E model is most applicable for correcting the E-region electron density peak concentrations in the auroral oval region. Two major improvements are envisioned in future model updates. The first is an extension of the model to latitudes equatorward of the auroral oval region. Figure 1 suggests large electron density gradients above the E-region peak at latitudes equatorward of the auroral oval for strong geomagnetic storms. The second major improvement is expanding the number of geomagnetic

activity indices to better predict storm-time enhancements of E-region electron densities in the polar cap region.

The initial version of STORM-E was compared to ISR electron density measurements at Tromso, Longyearsbyen, and Sondrestom during the Halloween 2003 storm events. Despite the fact that the available high-latitude ISR measurements are poleward of the main auroral oval region, STORM-E modestly to significantly improved the empirical model predictions of storm-time E-region electron densities. The model comparisons were made by scaling the nominal quiet-time IRI electron densities by the geomagnetic enhancement factor provided by STORM-E. Based on the storm-time IRI/ISR comparisons, the AE-index provided the best proxy for parameterizing geomagnetic enhancements in E-region electron densities. STORM-E driven by the AE-index improved the IRI/ISR comparisons by 20-60%. The worst proxy was Dst. STORM-E driven by the Dst-index improved the IRI/ISR comparisons by 5-44%. STORM-E performance poleward of the auroral oval region is expected to improve with the adoption of additional geomagnetic activity indices more suitable to the polar cap region.

Since the Ap-index is an IRI input already, integration of the initial version of STORM-E, parameterized by the Ap-index, into the IRI is rather straight forward. However, the results of this study prompt the IRI Working Group to consider incorporating additional geomagnetic indices, especially AE. Moreover, future updates to STORM-E may disclose the utility of the PC-index, or other derived geomagnetic activity indices. It is likely that geomagnetic parameterizations of other IRI outputs would benefit from the inclusion of AE and other solar-geomagnetic activity indices.

ACKNOWLEDGEMENTS

This material is based upon work supported by the National Aeronautics and Space Administration under grant NNH06DA001N issued through the Science Mission Directorate's Living With A Star Targeted Research and Technology Program.

REFERENCES

Araujo-Pradere, E. A., T. J. Fuller-Rowell, and D. Bilitza (2004), Time empirical ionospheric correction model (STORM) response in IRI2000 and challenges for empirical modeling in the future, *Radio Sci., 39,* RS1S24, doi:10.1029/2002RS002805.

Araujo-Padere, E. A., T. J. Fuller-Rowell, and D. Bilitza (2003), Validation of the STORM response in IRI2000, *J. Geophys. Res., 108(A3),* 1120, doi:10.1029/2002JA009720.

Araujo-Padere, E. A., T. J. Fuller-Rowell, and M. V. Codrescu (2002), STORM: An empirical storm-time ionospheric correction model 1. Model description, *Radio Sci., 37(5),* 1070, doi:10.1029/2001RS002467.

Bilitza, D. (2001), International Reference Ionosphere, *Radio Science., 36(2),* 261-265.

Burke, W. (2007), Interplanetary control of thermospheric densities during large magnetic storms, *J. Atmos. Solar-Terr. Phys., 69,* 279-287.

Fuller-Rowell, T. J., E. Araujo-Pradere, and M. V. Codrescu (2000), An empirical ionospheric storm-time correction model, *Adv. Space Res., 25(1),* 139-146.

Fernandez, J. R., C. J. Mertens, D. Bilitza, X. Xu, J. M. Russell III, and M. G. Mlynczak (2009), Storm/Quiet ratio comparisons between TIMED/SABER $NO^{+}(v)$ volume emission rates and incoherent scatter radar electron densities at E-region altitudes, submitted to *Adv. Space Res.* special issue on the International Reference Ionosphere.

Lyatsky, W., S. Lyatskaya, and A. Tan (2007), A coupling function for the solar wind effect on geomagnetic activity, *Geophy. Res. Lett., 34*, L02107, doi:10.1029/2006GL027666.

Mertens, C. J., J. M. Russell III, M. G. Mlynczak, C.-Y. She, F. J. Schmidlin, R. A. Goldberg, M. Lopez-Puertas, P. P. Wintersteiner, R. H. Picard, J. R. Winick, and X. Xu (2009a), Kinetic temperature and carbon dioxide from broadband infrared limb emission measurements taken from TIMED/SABER, *Adv. Space Res., 43*, 15-27.

Mertens, C. J., J. R. Winick, R. H. Picard, D. S. Evans, M. Lopez-Puertas, P. P. Wintersteiner, X. Xu, M. G. Mlynczak, and J. M. Russell III (2009b), Influence of solar-geomagnetic disturbances on SABER measurements of 4.3 um emission and the retrieval of kinetic temperature and carbon dioxide, *Adv. Space Res., 43*, 1325-1336.

Mertens, C. J., J. R. Fernandez, X. Xu, D. S. Evans, M. G. Mlynczak, and J. M. Russell III (2008), A new source of auroral infrared emission observed from TIMED/SABER, *Geophy. Res. Lett., 35*, L17106, doi:10.1029/2008GL034701.

Mertens, C. J., J. C. Mast, J. R. Winick, J. M. Russell III, M. G. Mlynczak, and D. S. Evans (2007a), Ionospheric E-region response to solar-geomagnetic storms observed by TIMED/SABER and application to IRI storm-model development, *Adv. Space Res., 39*, 715-728.

Mertens, C. J., J. R. Winick, J. M. Russell III, M. G. Mlynczak, D. S. Evans, D. Bilitza, and X. Xu (2007b), Empirical storm-time correction to the international reference ionosphere model E-region electron and ion density parameterizations using observations from TIMED/SABER, *Proceedings of SPIE, Remote Sensing of Clouds and the Atmosphere XII*, Florence, Italy, September 17-19, vol. 6745, 65451L, doi:10.1117/12.737318.

Vassiliadis, D., A. J. Klimas, S. G. Kanekal, D. N. Baker, and R. S. Weigel (2002), Long-term-average, solar cycle, and seasonal response of magnetospheric energetic electrons to the solar wind speed, *J. Geophys. Res., 107(A11),* 1383, doi:10.1029/2001JA000506.